RESEARCH ARTICLE

Thermal Modeling of the Ground Surface for the Purpose of Calculating the Current-Carrying Capacity of Underground Cable Lines Using the FEM

Dardan Klimenta[1], **Marko Šućurović**[2,*] **and Dragan Tasić**[3]

[1] Faculty of Technical Sciences, University of Priština in Kosovska Mitrovica, 38220 Kosovska Mitrovica, Serbia
[2] Faculty of Technical Sciences, University of Kragujevac, 32102 Čačak, Serbia
[3] Faculty of Electronic Engineering, University of Niš, 18104 Niš, Serbia

Abstract

In large-scale 2D finite element steady-state thermal models for underground cable ampacity calculations, where the lateral and lower boundaries are adiabatic, the ground surface may be represented by isothermal Dirichlet, convective Robin, or coupled convection–radiation conditions. In such cases, the soil temperature at depths significantly below the cables tends to be equal or to exceed the temperature of reference soil or air. This paper proposes a novel approach addressing this issue by dividing the native soil into two layers, introducing an effective thermal conductivity for the upper layer, and assuming distinct reference soil temperatures at the cable depth and at the lower boundary. The upper layer spans from the ground surface to the cable installation plane (where reference soil temperature is typically measured), while the lower layer extends to the domain's bottom. For summer periods, the effective thermal conductivity of the upper layer is calibrated to correspond to measured reference soil temperature under the most unfavorable environmental conditions. A temperature equal to the local average groundwater temperature is assigned to the lower boundary. The study focuses on AXLJ 1×1000/190 mm^2 110 kV cables in trefoil formation, installed in single- and two-layered native soils. Steady-state thermal analyses are performed using COMSOL 4.3. Results show that the cable ampacity can be increased by 8.43%, a value considered safe from both scientific and engineering perspectives.

Keywords: current-carrying capacity, finite element method (FEM), steady-state thermal modeling, underground cable line.

1 Introduction

Analytical calculation of the current-carrying capacity of any underground cable line in accordance with the IEC 60287 standards [1–3] involves using the temperature of the reference soil at the installation depth of that cable line [4, 5]. If the same current-carrying capacity is to be reproduced using the finite element method (FEM) in software such as

Submitted: 16 February 2026
Accepted: 20 March 2026
Published: 27 March 2026

Vol. 2, **No.** 1, 2026.
10.62762/TEPNS.2026.891956

***Corresponding author:**
✉ Marko Šućurović
marko.sucurovic@ftn.kg.ac.rs

Citation
Klimenta, D., Šućurović, M., & Tasić, D. (2026). Thermal Modeling of the Ground Surface for the Purpose of Calculating the Current-Carrying Capacity of Underground Cable Lines Using the FEM. *ICCK Transactions on Electric Power Networks and Systems*, 2(1), 47–57.

© 2026 ICCK (Institute of Central Computation and Knowledge)

COMSOL 4.3 [6], then the temperature of the reference soil at the installation depth of the underground cable line must be transformed into an isothermal Dirichlet boundary that should represent at least the ground surface [7–9]. If the ground surface temperature is equal to the temperature of the reference soil at the installation depth of the underground cable line, then the remaining three surfaces of the computational domain are usually represented by a thermally insulated Neumann boundary [7, 9]. In this case, the soil temperature at a greater distance from the power cables becomes equal or close to the temperature of Dirichlet boundary used to model the ground surface. When a convection Robin boundary is used for the ground surface instead of an isothermal Dirichlet boundary, the soil temperature at a greater distance from the power cables becomes equal or close to the temperature of air above the ground [9, 10]. Moreover, if a radiation boundary is also included, the temperature of the soil surrounding the power cables becomes higher than the temperature of air above the ground [11]. Consequently, under a Robin boundary condition of convection or the coupling of convection and radiation boundary conditions, the soil temperature at a significantly greater depth than that at which the cable line is installed can be close to, equal to or higher than the temperature of air above the ground, which is completely unrealistic and practically impossible.

Apart from References [9–11] and other publications by Klimenta, D. and his collaborators, there are not many research papers in the literature where the ground surface is represented by a convection Robin boundary or the coupling of convection and radiation boundary conditions. Among these papers, only a few can be singled out as relevant to the subject of research under consideration. For instance, in [12], it was assumed that the left-side, lower and right-side surfaces of a computational domain are thermally insulated, while the accompanying upper surface above underground power cables is isothermal at 20 °C. An analysis of the current-carrying capacity for an underground power cable considering a non-uniform temperature distribution over the ground surface (i.e., the coupling of two different isothermal Dirichlet boundary conditions) was conducted in [13]. In [14], the temperatures at the ground surface and the lower surface of the computational domain were set to be uniform and constant at the 25 °C and 20 °C in the summer period, respectively. In addition, a coupled natural convection-radiation boundary condition was used to model the ground surface above single- and double-circuit 110 kV underground cable lines in [15, 16]. Effects of environmental air and soil temperatures on heat transfer in underground power cables were analyzed in [17]. In this analysis, the ground surface is represented by a convection Robin boundary, the lower surface of a computational domain by an isothermal Dirichlet boundary, and the two lateral surfaces by a temperature distribution function [17], and so on. Therefore, only in Reference [17] it was concluded that the ground surface can be adequately represented by a convection Robin boundary only when the lower surface of the computational domain is represented by an appropriate isothermal Dirichlet boundary. Based on the literature review, it is obvious that most existing studies of this type do not take into account the matching of simulated and measured temperatures of the reference soil at the cable installation depth, as well as the effect of the overall heat transfer at the ground surface. This is recognized as a research gap that needs to be addressed.

This paper addresses the recognized research gap through examples of three 110 kV single-core cables of the type AXLJ 1×1000/190 mm^2 installed directly in the single- and two-layered native soils, assuming that the upper layer is completely dried-out and the lower layer is not. The single-layered native soil will be used in three IEC- and FEM-based simulations with a 40 m wide and 21.5 m deep computational domain – large-scale domain, different boundary conditions at the ground surface, and the current-carrying capacity corresponding to a continuously permissible temperature of 90 °C – for cross-linked polyethylene (XLPE)-insulated cables. The results of these simulations serve to identify the existence of unrealistic details in the generated temperature distributions. Then, a series of FEM-based simulations will be performed with a 10 m wide and 5 m deep computational domain – small-scale domain (created in accordance with IEC TR 62095), de-energized power cables, and a two-layered native soil, assuming that the thermal conductivity of the lower native soil layer is known. In addition, during the summer periods, the upper layer of the native soil cracks and becomes a complex combination of various air cracks (with a thermal conductivity of 0.025 W/(mK)) and irregular soil blocks (for instance, with a thermal conductivity of 1 W/(mK)). The resulting thermal conductivity of such a soil layer is unknown and can be defined as the effective thermal conductivity. The purpose of the series of simulations

with the small-scale domain is to determine the effective thermal conductivity of the upper native soil layer under the condition that the temperature of the reference soil at the cable installation depth is equal to the measured value of 20 °C [4, 5]. The last series of simulations is performed with the same small-scale domain but with the aim of determining the current-carrying capacity at the continuously permissible temperature of XLPE-insulated cables. In all simulations, it is assumed that the 110 kV cables are run in trefoil formation, as well as operate under balanced three-phase loads and the most unfavorable environmental conditions. The thermal analysis of the underground power cables in a steady-state is performed using the FEM in COMSOL 4.3 Heat Transfer Module [6]. The proposed approach is novel, easy, user-friendly and consists of (i) dividing the native soil into two layers; (ii) determining the effective thermal conductivity for the upper native soil layer under the condition that the temperature of the reference soil at the cable installation depth is equal to the corresponding measured value; (iii) modeling of the ground surface with a coupled convection-radiation boundary condition; and (iv) modeling of the lower surface of the small-scale domain with a constant temperature equal to the average temperature of drinking water from Serbian groundwater sources. The given features represent the original and innovative solutions. The accuracy of the FEM-based steady-state thermal model having a reduced geometry (10 m 5 m) was verified by means of finite element (FE) mesh convergence tests.

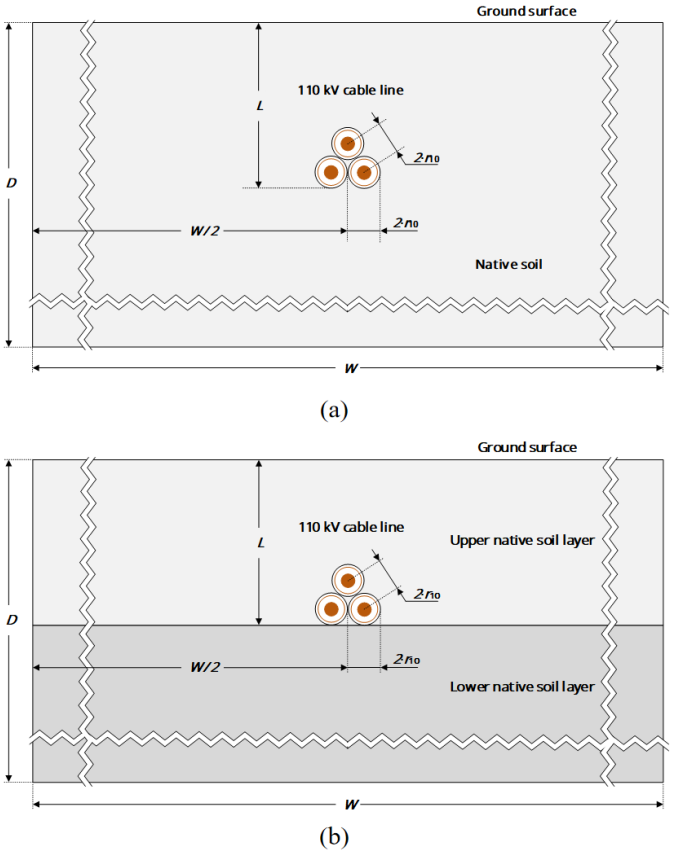

Figure 1. Representation of the large- and small-scale domains with single-core 110 kV cables of the type AXLJ 1×1000/190 mm^2 installed directly in the native soil in trefoil formation; (a) large-scale domain with single-layered native soil; and (b) small-scale domain with two-layered native soil.

2 Problem Formulation

To illustrate the thermal effects of different boundary conditions at the ground surface on the native soil surrounding 110 kV cables and the cables themselves, the computational domains in Figure 1(a, b) will be considered. The parameters shown in Figure 1 are as follows: D is the depth of the large- or small-scale domain in m, W is the width of the large- or small-scale domain in m, $L = 1.5$ m is the cable line installation depth, and r_{10} is the radius of a single 110 kV cable in m.

The large-scale domain in Figure 1(a) has dimensions of 40 m × 21.5 m, single-layered and moderately dried-out native soil, thermally insulated boundaries on the left-side, lower and right-side surfaces, and the ground surface represented by: (i) a constant temperature equal to the temperature of the reference soil at the installation depth of the underground cable line – the first simulation; (ii) the coupling of convection and surface-to-environment radiation boundary conditions – the second simulation; and (iii) the coupling of convection, received heat flux and radiated heat flux boundary conditions – the third simulation. The first simulation is organized to comply with the IEC 60287 standards [1–3] and to give the current-carrying capacity very close to that obtained by the IEC-based analytical procedure. Compared to the first simulation, the second and third simulations differ only in the way the ground surface is modeled. These three simulations were prepared with the aim of showing that the temperatures of the native soils surrounding power cables are unrealistic and practically impossible, that each simulation provides different current-carrying capacity, and that FEM-based steady-state thermal models do not necessarily generate solutions identical to those of the Neher-McGrath method used by the IEC 60287 standards [1–3]. Specifically, it will be determined whether there are certain increases in the temperature

of the reference soil at the cable installation depth compared to the corresponding measured value, as well as whether there are certain reductions in the current-carrying capacity compared to the value obtained by applying the analytical procedure based on IEC 60287. After these three simulations, a temperature distribution and a current-carrying capacity of the cables that make physical sense should be generated using the small-scale domain from Figure 1(b).

The small-scale domain in Figure 1(b) has dimensions of 10 m × 5 m, two-layered native soil, thermally insulated boundaries on the left- and right-side surfaces, an isothermal Dirichlet boundary on the lower surface, and the ground surface represented by the coupling of convection, received heat flux and radiated heat flux boundary conditions. This domain is created in accordance with IEC TR 62095 and is used for: (i) simulations with de-energized 110 kV cables and a known thermal conductivity of the lower native soil layer – the first series of simulations for determining the effective thermal conductivity of the upper native soil layer; and (ii) simulations with energized power cables and thermal conductivities of the two native soil layers determined in the first series of simulations – the second series of simulations for determining the current-carrying capacity of the underground cable line. In both domains, single-core 110 kV cables of the type AXLJ $1 \times 1000/190$ mm^2 are installed in trefoil formation, directly in the native soil.

Each cable of the type AXL 1×1000/190 mm² 110 kV consists of ten construction elements in the shape of solid and hollow cylinders. The radii of these cylindrical elements are as follows: $r_1 = 0.0192$ m – radius of aluminum conductor, $r_2 = 0.02095$ m – outer radius of semi-conductive XLPE screen covering the conductor, $r_3 = 0.03405$ m – outer radius of XLPE insulation, $r_4 = 0.03505$ m – outer radius of semi-conductive XLPE screen covering the insulation, $r_5 = 0.03565$ m – outer radius of semi-conductive polyethylene (PE) tapes beneath the copper screen, $r_6 = 0.03755$ m – outer radius of copper screen having a rated cross-section of 190 mm², $r_7 = 0.03815$ m – outer radius of semi-conductive PE tapes covering the copper screen, $r_8 = 0.03835$ m – outer radius of radial water-sealing aluminum layer, $r_9 = 0.03855$ m – outer radius of conductive high density polyethylene (HDPE) layer, and $r_{10} = 0.04215$ m – outer radius of HDPE sheath. According to [1, 9], each 110 kV cable needs to be represented by an equivalent design consisted of the aluminum conductor, XLPE insulation, copper screen and HDPE sheath with outer radii equal to those of the first, fifth, eighth and tenth cylindrical layer of the actual AXL 1×1000/190 mm² 110 kV cable construction, respectively. Specifically, the semi-conductive conductor and insulation screens and PE tapes beneath the copper screen are included in equivalent XLPE insulation with a thermal conductivity of $k_5 = 0.286\,\mathrm{W/(K{\cdot}m)}$; the PE tapes covering the copper screen and water-sealing aluminum layer are added to an equivalent copper screen with a thermal conductivity of $k_8 = 385\,\mathrm{W/(K{\cdot}m)}$; while the conductive HDPE layer is incorporated in an equivalent HDPE sheath with a thermal conductivity of $k_{10} = 0.245\,\mathrm{W/(K{\cdot}m)}$ [9]. Thermal conductivity of the aluminum conductors is assumed to be $k_1 = 239\,\mathrm{W/(K{\cdot}m)}$ [9]. Since the PE tapes covering the copper screen are added to the equivalent copper screen, it means that their thermal conductivity was taken into account by the thermal conductivity of the equivalent HDPE sheath k_{10} [10].

The copper screens are assumed to be cross-bonded, while the phase currents are assumed to be mutually equal and balanced. This means that there will be no heat generation in the equivalent copper screens. Accordingly, heat generation will exist in the conductors and equivalent insulation layers. Although IEC 60287-1-1 [1] recommends to ignore dielectric losses for the line voltages up to and including 110 kV, they are used in all FEM-based calculations. Logically, only the electric resistivity of aluminum conductors at 20 °C (i.e., $\rho_{Al} = 2.8264 \cdot 10^{-8}\,\Omega{\cdot}\mathrm{m}$) is necessary for the calculation of the power of volumetric heat generation in the conductors. Based on [9], the current-carrying capacity, power of volumetric heat generation in the conductors and power of volumetric heat generation in the insulation layers calculated according to IEC 60287 [1–3] are $I = 593.972$ A, $Q_{c,v} = 12496.5\,\mathrm{W/m^3}$ and $Q_{d,v} = 127.936\,\mathrm{W/m^3}$, respectively.

The most unfavorable environmental conditions which will be used here are as follows [9, 11]: (i) temperature of air above the ground $T_a = 40\,^\circ\mathrm{C}$; (ii) solar irradiance $Q_{S,s} = 1000\,\mathrm{W/m^2}$; (iii) temperature of the reference soil at the installation depth of the given cable line $T_{rs} = 20\,^\circ\mathrm{C}$; (iv) temperature of the reference soil below the cable line $T'_{rs} = 20\,^\circ\mathrm{C}$; (v) thermal conductivity of the native soil in a normal state $k_{ns} = 1\,\mathrm{W/(K{\cdot}m)}$; and (vi) thermal conductivity of the native soil in a moderately dried-out state $k_{ns} = 0.4\,\mathrm{W/(K{\cdot}m)}$. In addition, the ground surface is assumed to be covered with dry grass. Radiation properties of such ground surface

are $\varepsilon = 0.94$ – thermal emissivity and $\alpha = 0.6$ – solar absorptivity [11]. It is also assumed that the heat transfer coefficient by convection is $h_c = 12.654\,\mathrm{W/(m^2{\cdot}K)}$ [11].

3 Steady-State Thermal Analysis

Steady-state thermal analyses of the large- and small-scale two-dimensional domains in Figure 1 using the FEM are governed by the following equation [9–11]:

$$\nabla \cdot (-k\nabla T) = Q_v \tag{1}$$

where k is the thermal conductivity in W/(K·m); T is the unknown nodal temperature in K; ∇T is the temperature gradient consisting of partial derivatives of the variable T with respect to the abscissa x and the ordinate y in the Cartesian coordinate system in m; and Q_v is the power of volumetric heat generation in $\mathrm{W/m^3}$.

If there is any radiation boundary in each of these FEM-based models, the model is nonlinear, otherwise the model is linear.

The power of volumetric heat generation in three conductors with a radius of $r_1 = 0.0192\,\mathrm{m}$ and a geometric cross-section of $S'_c = 1158.117 \cdot 10^{-6}\,\mathrm{m^2}$ [9,11]:

$$Q_{c,v} = \frac{R_{ac}(T_{cp})}{S'_c} I^2 \tag{2}$$

where $R_{ac}(T_{cp}) = 4.102127 \cdot 10^{-5}\,\Omega/\mathrm{m}$ is the AC resistance of a single conductor per unit length at temperature T_{cp}, calculated based on IEC 60287-1-1 [1] and IEC 60228 [18]; $T_{cp} = 90°\,\mathrm{C}$ is the continuously permissible temperature of XLPE cables; and I is the current-carrying capacity or load current in A.

The power of volumetric heat generation in three equivalent insulation layers is given by [9, 11]:

$$Q_{d,v} = \frac{Q_{d,l}}{\pi(r_5^2 - r_1^2) \cdot 10^{-6}} \tag{3}$$

where $Q_{d,l} = 0.362647\,\mathrm{W/m}$ is the dielectric loss per unit length, and $\pi(r_5^2 - r_1^2) \cdot 10^{-6}$ is the geometric cross-section of a single equivalent insulation layer in $\mathrm{m^2}$.

3.1 Modeling of Boundaries According to IEC TR 62095

According to IEC TR 62095 [7], the ground surface in the large- and small-scale domains in Figure 1 can be represented by

$$T = T_{rs} \tag{4}$$

– isothermal Dirichlet boundary, or

$$\vec{n} \cdot (-k\nabla T) = h_c(T - T_a) \tag{5}$$

– convection Robin boundary. In addition to this, the left-side, lower and right-side surfaces of the large-scale domain in Figure 1(a) are represented by

$$\vec{n} \cdot (-k\nabla T) = 0 \tag{6}$$

– Neumann boundary of thermal insulation [7, 9–11]. In these boundary conditions, T is the unknown temperature of the domain surfaces in K; T_{rs} is the temperature of the ground surface in K; T_a is the temperature of air above the ground in K; $\vec{n}$ is the outwards-oriented normal vector of the Robin and Neumann boundaries; and h_c is the heat transfer coefficient by convection in $\mathrm{W/(m^2{\cdot}\,K)}$. In the first simulation, a combination of boundary conditions (4) and (6) will be applied.

3.2 Proposed Modeling of Boundaries

The ground surface in the large- and small-scale domains in Figure 1 can also be represented by the coupling of the following boundary conditions:

$$\vec{n} \cdot (-k\nabla T) = \varepsilon \cdot \sigma_{SB} \cdot (T^4 - T_a^4) \tag{7}$$

– surface-to-environment radiation boundary condition [9, 11] and convection Robin boundary condition given by Equation (5). Otherwise, the ground surface can be represented by the coupling of

$$\vec{n} \cdot (-k\nabla T) = -\alpha \cdot Q_{S,s} \tag{8}$$

– received heat flux boundary condition,

$$\vec{n} \cdot (-k\nabla T) = \varepsilon \cdot \sigma_{SB} \cdot T^4 \tag{9}$$

– radiated heat flux boundary condition, and convection Robin boundary condition given by Equation (5) [9, 11]. In the second and third simulations, the left-side, lower and right-side surfaces of the large-scale domain in Figure 1(a) will be represented by the Neumann boundary condition of thermal insulation, that is, Equation (6). While in the remainder of the simulations with the small-scale domain in Figure 1(b), the left- and right-side surfaces will be represented by the Neumann boundary

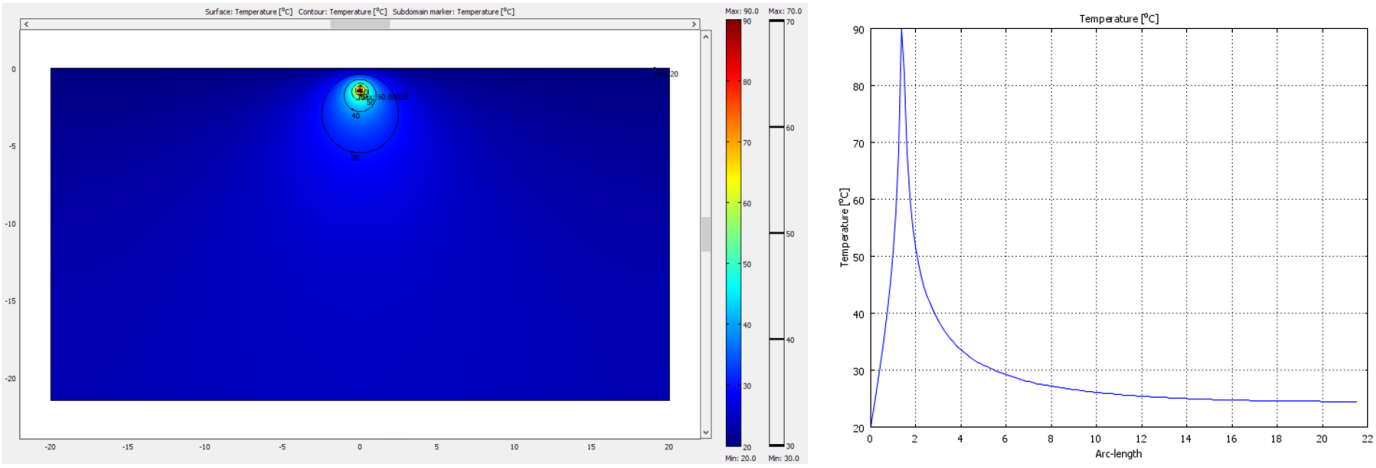

(a) (b)

Figure 2. Results of the first simulation with the large-scale domain generated for the ground surface modeled in accordance with IEC 60287 by the isothermal Dirichlet boundary condition (4); (a) Temperature distribution and isotherms of 30, 40, 50, 60 and 70 °C; and (b) Temperature distribution along the vertical axis of symmetry of the large-scale domain.

condition of thermal insulation, and the lower surface by

$$T = T'_{rs} \tag{10}$$

– an isothermal Dirichlet boundary condition, where T'_{rs} stands for the temperature of the reference soil below the cable line in K. In Equations (7), (8) and (9), $\vec{n}$ is the outwards-oriented normal vector of the radiation boundaries and $\sigma_{SB} = 5.67 \cdot 10^{-8}\,\mathrm{W/(m^2 \cdot K^4)}$ is the Stefan-Boltzmann constant, while the other parameters and variables were already defined. In addition, it is assumed that the temperature of the reference soil below the cable line is equal to the average temperature of drinking water from groundwater sources in Serbia, that is, $T'_{rs} = 8°\mathrm{C}$.

4 Results and Observations

4.1 The First Simulation with the Large-Scale Computational Domain

Figure 2(a) presents the temperature distribution over the large-scale domain generated for the ground surface modeled in accordance with IEC 60287 by the isothermal Dirichlet boundary condition (4). Here, the ground surface is assumed to be an isotherm whose temperature is equal to the temperature of the reference soil at the installation depth of the considered cable line. Figure 2(a) also shows the isotherms of 30, 40, 50, 60 and 70 °C. In addition, Figure 2(b) presents the temperature distribution along the vertical axis of symmetry of the large-scale domain.

The results of this simulation are as follows: power of volumetric heat generation in the conductors $Q_{c,v} = 12430.8\,\mathrm{W/m^3}$, current-carrying capacity $I = 592.408\,\mathrm{A}$, and temperature at the point of intersection between the lower surface and the vertical axis of symmetry of the considered computational domain $T_{r,s,FEM} = 24.5\,°\mathrm{C}$. These results correspond to the continuously permissible temperature of XLPE cables $T_{cp} = 90\,°\mathrm{C}$.

The main observations from Figure 2(a, b) indicate the following: (i) The current-carrying capacity calculated using the FEM-based model differs from the one calculated using the corresponding IEC-based model by -1.564 A or -0.263 % [9]. (ii) The simulated temperature of the reference soil at the installation depth of the considered cable line is very close to the corresponding measured value of 20 °C. (iii) The simulated temperature of the reference soil at the lower surface of the large-scale domain below the considered cable line (in the direction of the vertical axis of symmetry) is 4.5 °C higher than the ground surface temperature, which is unrealistic and practically impossible.

4.2 The Second Simulation with the Large-Scale Computational Domain

Figure 3(a) shows the temperature distribution over the large-scale domain obtained for the ground surface represented by the coupling of boundary conditions (5) and (7), while Figure 3(b) shows the temperature distribution along the vertical axis of symmetry of the large-scale domain.

For $T_{cp} = 90\,°\mathrm{C}$, the second simulation resulted in: $Q_{c,v} = 8760.2\,\mathrm{W/m^3}$, $I =$

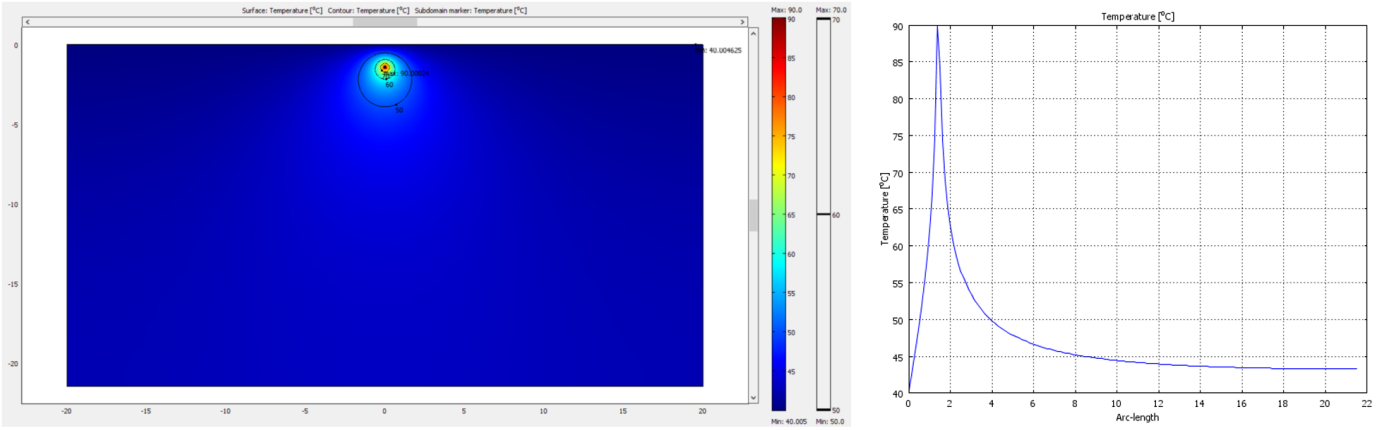

(a) (b)

Figure 3. Results of the second simulation with the large-scale domain generated for the ground surface modeled by the coupling of convection and surface-to-environment radiation boundary conditions using Equations (5) and (7), respectively; (a) Temperature distribution and isotherms of 50, 60 and 70 °C; and (b) Temperature distribution along the vertical axis of symmetry of the large-scale domain.

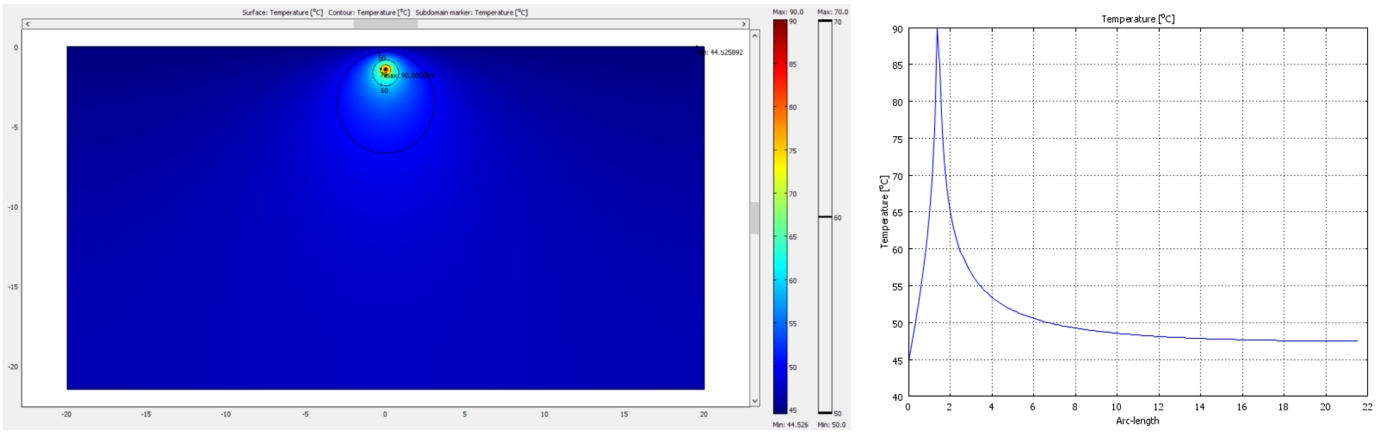

(a) (b)

Figure 4. Results of the third simulation with the large-scale domain generated for the ground surface modeled by the coupling of convection, received heat flux and radiated heat flux boundary conditions using Equations (5), (8) and (9), respectively; (a) Temperature distribution and isotherms of 50, 60 and 70 °C; and (b) Temperature distribution along the vertical axis of symmetry of the large-scale domain.

497.312 A, and $T'_{rs,FEM} = 43.3\,^{\circ}\text{C}$.

The main observations from Figure 3 indicate the following: (i) The current-carrying capacity obtained using the FEM differs from the corresponding IEC-based value by −96.66 A or −16.273 %. (ii) The simulated temperature of the reference soil at the cable installation depth is very close to the temperature of air above the ground. (iii) The simulated temperature of the reference soil at the lower boundary below the considered cable line is 3.3 °C higher than the temperature of air above the ground. The observations (ii) and (iii) are unrealistic and physically impossible.

4.3 The Third Simulation with the Large-Scale Computational Domain

The temperature distribution over the large-scale domain obtained for the ground surface represented by the coupling of boundary conditions (5), (8) and (9) is shown in Figure 4a. In addition, the temperature distribution along the vertical axis of symmetry of the same domain is shown in Figure 4b.

For $T_{cp} = 90\,^{\circ}\text{C}$, the third simulation provided: $Q_{c,v} = 7941.3\,\text{W/m}^3$, $I = 473.497\,\text{A}$, $T'_{rs,FEM} = 47.5\,^{\circ}\text{C}$.

Three major observations from Figure 4 are as follows: (i) The FEM-based current-carrying capacity differs from the corresponding IEC-based current-carrying capacity by −120.475 A or −20.283 %. (ii) The simulated value of the reference soil temperature at the

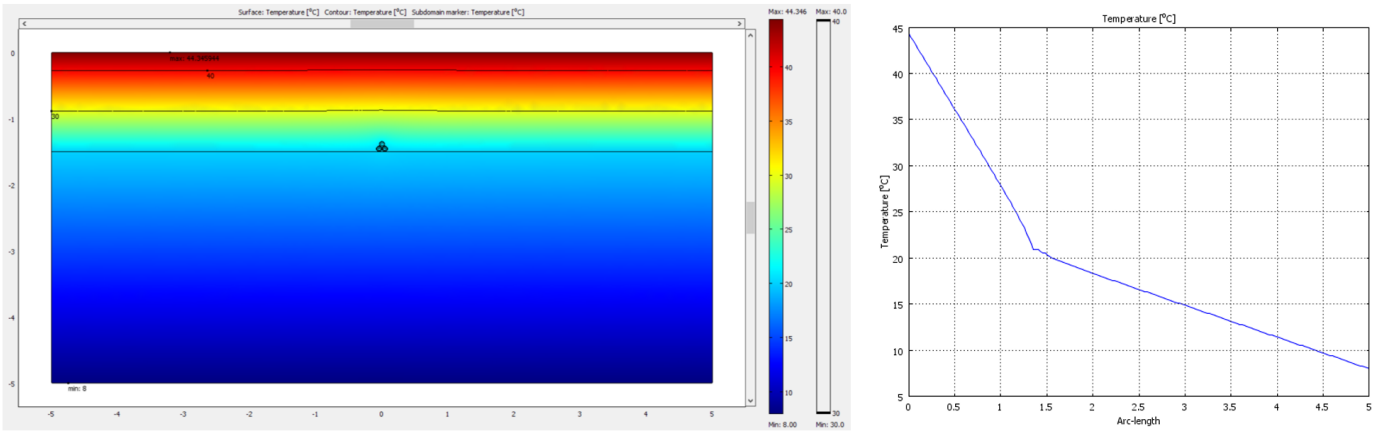

(a) (b)

Figure 5. Final results of the first series of simulations with the small-scale domain generated for de-energized power cables and the ground surface modeled by the coupling of convection, received heat flux and radiated heat flux boundary conditions using Equations (5), (8) and (9), respectively; (a) Temperature distribution and isotherms of 30 and 40 °C; and (b) Temperature distribution along the vertical axis of symmetry of the small-scale domain.

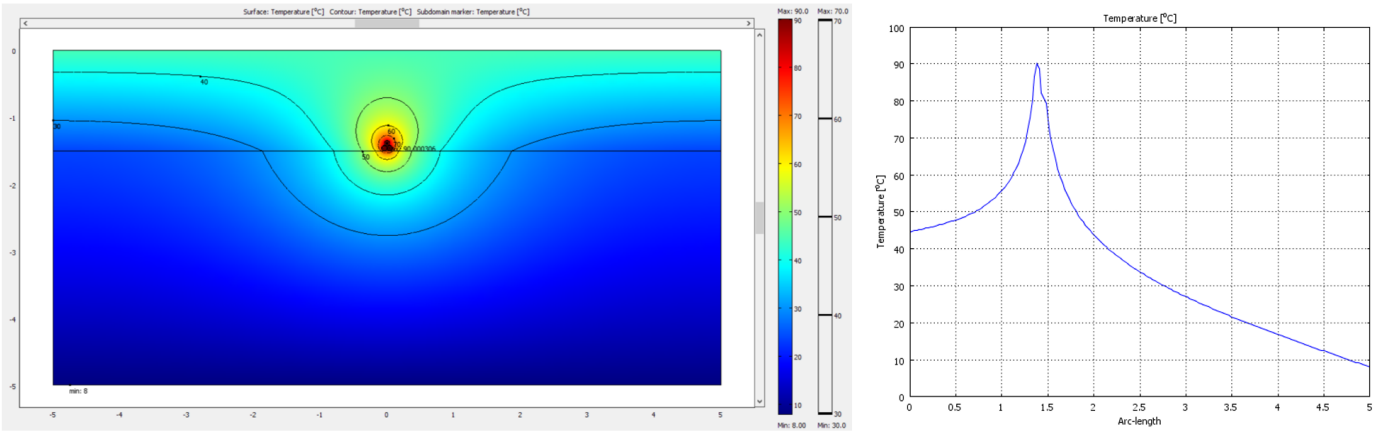

(a) (b)

Figure 6. Final results of the second series of simulations with the small-scale domain generated for energized power cables and the ground surface modeled by the coupling of convection, received heat flux and radiated heat flux boundary conditions using Equations (5), (8) and (9), respectively; (a) Temperature distribution and isotherms of 30, 40, 50, 60 and 70 °C; and (b) Temperature distribution along the vertical axis of symmetry of the small-scale domain.

cable installation depth is higher than the temperature of air above the ground. (iii) The simulated value of the reference soil temperature at the lower boundary below the considered cable line is 7.5 °C higher than the temperature of air above the ground. And again the second and third observations are unrealistic and impossible.

4.4 The First Series of Simulations with the Small-Scale Computational Domain

Figure 5(a, b), respectively, show the temperature distributions over the small-scale domain and along its vertical axis of symmetry generated for de-energized power cables, the thermal conductivity of the lower native soil layer $k_{ns} = 1\,\mathrm{W/(K{\cdot}m)}$, the ground surface represented by the coupling of boundary conditions (5), (8) and (9), and the lower surface of the small-scale domain represented by the boundary condition (10).

The first series of simulations with the small-scale domain resulted in the effective thermal conductivity of the upper native soil layer of 0.211 W/(K·m).

The major observation from Figure 5 is: The simulated value of the reference soil temperature at the cable installation depth $L = 1.5\,\mathrm{m}$ is equal to the corresponding measured value $T_{rs} = 20\,^{\circ}\mathrm{C}$. This result can be regarded as realistic and practically possible, which makes it logical to model the lower surface of the small-scale domain with the isothermal Dirichlet boundary condition (10). This approach also found an experimental background in the results

Table 1. Results of FE mesh convergence tests performed using the FEM-based steady-state thermal model from Figure 1(b).

FE mesh	Number of nodes	Number of finite elements	Conductor temperature in °C	Conductor temperature deviation in °C
Default generation	2717	5375	90.000306	-
After the first refinement	10808	21500	90.002912	+0.002606
After the second refinement	43115	86000	90.003027	+0.002721

reported in [17]. Specifically, in [17] it was pointed out that the temperature of air above the ground strongly affects the soils up to a depth of 3.6 m.

4.5 The Second Series of Simulations with the Small-Scale Computational Domain

The temperature distributions over the small-scale domain and along its vertical axis of symmetry generated for energized power cables and other service conditions identical to those from the first series of simulations with this small-scale domain are shown in Figure 6.

The second series of simulations with this domain resulted in: $Q_{c,v} = 14231.4\,\mathrm{W/m^3}$ and $I = 633.863\,\mathrm{A}$.

Two major observations from Figure 6 are: (i) The simulated temperature of the reference soil at the installation depth $L = 1.5\,\mathrm{m}$ is equal to $T_{rs} = 20°\mathrm{C}$. (ii) The FEM-based current-carrying capacity is 39.891 A or 8.84 % higher than the corresponding IEC-based current-carrying capacity. Both these observations are realistic and practically possible.

4.6 Finite Element Mesh Convergence Tests

Table 1 provides the results of FE mesh convergence tests performed using the FEM-based thermal model whose geometry is shown in Figure 1(b) for the service conditions considered in Section 4.5. The density of FE mesh generated within the small-scale computational domain was varied from the density associated with default mesh generation to the densities associated with the first two refinements. The convergence tests were conducted in accordance with [9–11], and the conductor temperatures were tracked. The differences between every two successive conductor temperatures were lower than 0.003 °C. Accordingly, the variations in the FE mesh density do not affect the conductor temperature and the corresponding current-carrying capacity. Therefore, the automatic mesh generation feature of COMSOL 4.3 provided temperature distributions with satisfactory accuracy.

5 Conclusion

The key conclusions that can be drawn on the basis of the presented results and main observations are:

- The convection Robin boundary recommended by IEC TR 62095 for modeling the ground surface in FEM-based current-carrying capacity calculations of underground cable lines can only be applied if the lower surface of any computational domain is represented by an appropriate isothermal Dirichlet boundary and if the vertical dimension of that computational domain is not less than 5 m.
- If FEM-based calculations of the current-carrying capacity require that the ground surface above underground power cables be represented by the coupling of convection and radiation boundary conditions, then the lower surface of a computational domain should also be set at a depth of 5 m and represented by an appropriate isothermal Dirichlet boundary.
- By dividing the native soil into two layers and introducing the effective thermal conductivity for the upper native soil layer into FEM-based calculations of the current-carrying capacity for underground cable lines, it is ensured that the reference soil temperature at the cable installation depth can be equal to the corresponding measured value, and that temperature distributions over a computational domain make physical sense.
- The assumption that the temperature of the reference soil beneath an underground cable line is constant and equal to the average temperature of drinking water from Serbian groundwater sources is physically absolutely correct, in compliance with the relevant experimental results of previous studies, and applicable to any other region or urban area.
- The proposed FEM-based approach showed that the current-carrying capacity of the considered 110 kV underground cable line can be 8.43 % higher than that calculated by the traditional

analytical procedure based on IEC 60287.

Finally, future research should address the application of the proposed approach to the FEM-based calculations of the current-carrying capacity for underground cable lines installed in various bedding materials and at different depths. In addition, the generalization of the proposed approach to cases of all other seasons should be considered.

Data Availability Statement

Data will be made available on request.

Funding

This work was supported by the Government of the Republic of Serbia under Grant 451-03-34/2026-03/200155, Grant 451-03-34/2026-03/200132, and Grant 451-03-34/2026-03/200102.

Conflicts of Interest

The authors declare no conflicts of interest.

AI Use Statement

The authors declare that no generative AI was used in the preparation of this manuscript.

Ethical Approval and Consent to Participate

Not applicable.

References

[1] International Electrotechnical Commission. (2023). Electric cables – Calculation of the current rating – Part 1-1: Current rating equations (100 % load factor) and calculation of losses – General (Standard IEC 60287-1-1:2023 CMV). *IEC*. Retrieved from https://webstore.iec.ch/en/publication/85666

[2] International Electrotechnical Commission. (2023). Electric cables – Calculation of the current rating – Part 2-1: Thermal resistance – Calculation of thermal resistance (Standard IEC 60287-2-1:2023 CMV). *IEC*. Retrieved from https://webstore.iec.ch/en/publication/85669

[3] International Electrotechnical Commission. (2017). Electric cables – Calculation of the current rating – Part 3-1: Operating conditions – Site reference conditions (Standard IEC 60287-3-1:2017 RLV). *IEC*. Retrieved from https://webstore.iec.ch/en/publication/60845

[4] Sredojevic, M. R., Naumov, R. M., Popovic, D. P., & Simie, M. D. (1997, June). Long term investigation of thermal behaviour of 110 kV underground transmission lines in the Belgrade area. In *14th International Conference and Exhibition on Electricity Distribution. Part 1. Contributions* (*IEE Conf. Publ. No. 438*) (Vol. 3, pp. 44-1). IET. [CrossRef]

[5] Sredojevic, M. R., Popovic, D. P., & Simic, M. D. (1999, August). Permissible current rating of the investigated 110 kV underground cable line. In *PowerTech Budapest 99. Abstract Records.*(*Cat. No. 99EX376*) (p. 218). IEEE. [CrossRef]

[6] COMSOL. (2012). *COMSOL Multiphysics user's guide* (Version 4.3) [Computer software]. COMSOL Inc.

[7] International Electrotechnical Commission. (2003). Electric cables – Calculations for current ratings – Finite element method (Technical Report IEC TR 62095:2003). *IEC*. Retrieved from https://webstore.iec.ch/en/publication/6455

[8] CIGRE Working Group B1.87. (2025). *Finite element analysis for cable rating calculations* (Technical Brochure TB 963). CIGRE. Retrieved from https://www.e-cigre.org/publications/detail/963-finite-element-analysis-for-cable-rating-calculations.html#pSummary

[9] Klimenta, D., Šućurović, M., & Tasić, D. (2025). Amendments to some IEC TR 62095 recommendations for underground single-core power cables in trefoil formation. *ICCK Transactions on Electric Power Networks and Systems*, *1*(1), 38–49. [CrossRef]

[10] Šućurović, M., Klimenta, D., & Tasić, D. (2024). Correction of the iec formula for the eddy-current loss factor: The case of single-core cables in trefoil formation with metallic screens bonded and earthed at one end. *Facta Universitatis, Series: Electronics and Energetics*, *37*(2), 391-408. [CrossRef]

[11] Klimenta, D., Perović, B., Klimenta, J., Jevtić, M., Milovanović, M., & Krstić, I. (2018). Controlling the thermal environment of underground cable lines using the pavement surface radiation properties. *IET Generation, Transmission & Distribution*, *12*(12), 2968-2976. [CrossRef]

[12] Rerak, M., & Ocłoń, P. (2017). Thermal analysis of underground power cable system. *Journal of Thermal Science*, *26*(5), 465-471. [CrossRef]

[13] Maximov, S., Venegas, V., Guardado, J. L., Moreno, E. L., & López, R. (2016). Analysis of underground cable ampacity considering non-uniform soil temperature distributions. *Electric Power Systems Research*, *132*, 22–29. [CrossRef]

[14] M'hamed, B., Ali, K. S., Leila, M. S., Sidik, N. A. C., Japar, W. M. A. A., & Mohamad, A. T. (2014). Thermal state effects on potential augmentation of the ampacity of a medium voltage underground cable in power distribution: A case study. *Journal of Advanced Research in Numerical Heat Transfer*, *18*(1), 1–13.

[15] Nahman, J., & Tanaskovic, M. (2013). Calculation of the ampacity of high voltage cables by accounting for radiation and solar heating effects using FEM.

International Transactions on Electrical Energy Systems, *23*(3), 301-314. [CrossRef]

[16] Nahman, J., & Tanaskovic, M. (2011). Evaluation of the loading capacity of a pair of three-phase high voltage cable systems using the finite-element method. *Electric Power Systems Research*, *81*(7), 1550–1555. [CrossRef]

[17] Kim, Y.-S., Cong, H. N., Dinh, B. H., & Kim, H.-K. (2025). Effect of ambient air and ground temperatures on heat transfer in underground power cable system buried in newly developed cable bedding material. *Geothermics*, *125*, 103151. [CrossRef]

[18] International Electrotechnical Commission. (2023). Conductors of insulated cables (Standard IEC 60228:2023 CMV). *IEC*. Retrieved from https://webstore.iec.ch/en/publication/90329

Dardan Klimenta was born in Serbia, in 1975. He graduated from the Faculty of Electrical Engineering, University of Priština, in 1998. Also, he received his postgraduate M.Sc. and Ph.D. in 2001 and 2007, respectively, from the Faculty of Electrical Engineering, University of Belgrade. His main research interests include electrical power cable engineering, renewable energy sources, electric power system components, heat transfer, optimization methods, FEM and FEA. Currently, he is a Full Professor with the Faculty of Technical Sciences, University of Priština in Kosovska Mitrovica. (Email: dardan.klimenta@pr.ac.rs)

Marko Šućurović was born in Serbia, in 1988. He received his B.Sc. and M.Sc. in 2011 and 2012, respectively, from the Faculty of Technical Sciences in Čačak, University of Kragujevac. Also, he is a Ph.D. student at the Faculty of Electronic Engineering, University of Niš. His main research interests include electrical power cable engineering, renewable energy sources, electric power system components, heat transfer, FEM and FEA. Currently, he is a Teaching and Research Assistant with the Faculty of Technical Sciences in Čačak, University of Kragujevac. (Email: marko.sucurovic@ftn.kg.ac.rs)

Dragan Tasić was born in Serbia, in 1961. He graduated from the Faculty of Electrical Engineering, University of Belgrade, in 1986. Also, he received his postgraduate M.Sc. in 1991 from the Faculty of Electrical Engineering, University of Belgrade, and Ph.D. in 1997 from Faculty of Electronic Engineering, University of Niš. His main research interests include electrical power cable engineering, renewable energy sources, electric power system modeling and analysis, heat transfer and optimization methods. Currently, he is a Full Professor with the Faculty of Electronic Engineering, University of Niš. (Email: dragan.tasic@elfak.ni.ac.rs)